Comparison of GNSS Multipath/NLoS Characterization Between Geodetic Receivers and Smartphones Across GPS L1 C/A and L5 Signals

Comparison of GNSS Multipath/NLoS Characterization Between Geodetic Receivers and Smartphones across GPS L1 C/A and L5 Signals

Yihan Guo [1], Simone Zocca [1], Paolo Dabove [2], Fabio Dovis [1]

[1] *Department of Electronics and Telecommunications (DET), Politecnico di Torino (Turin, Italy)*
[2] *Department of Environment, Land and Infrastructure Engineering (DIATI), Politecnico di Torino (Turin, Italy)*

BIOGRAPHY

Yihan Guo received the B.Sc. degree from Northwestern Polytechnical University, China, in 2016, and the M.Sc. degree from Shanghai Jiaotong University, China, in 2019. He is a Ph.D. student at the Department of Electronics and Telecommunications (DET) of Politecnico di Torino, Turin, Italy, and a member of the Navigation Signal Analysis and Simulation - NavSAS - group. His current research interests include integrated navigation systems and the techniques for detecting and mitigating GNSS multipath/NLoS interference.

Simone Zocca received a B.Sc. in Telecommunication Engineering in 2018 and a M.Sc. in Communication and Computer Networks Engineering in 2020, both from Politecnico di Torino, Turin, Italy. He is currently a Ph.D. student within the Navigation Signal Analysis and Simulation - NavSAS - group at the Department of Electronics and Telecommunications (DET) of Politecnico di Torino. His research is focused on innovative solutions for signal processing techniques and Bayesian estimation applied to Global Navigation Satellite System (GNSS).

Paolo Dabove received the M.Sc. from the University of Genoa and Ph.D. degrees from the Politecnico di Torino, Turin, Italy, in 2009 and 2013, respectively. In 2010, he joined the Department of Environment, Land and Infrastructure Engineering, where he has been an Associate Professor since 2021. His research activity is mainly focused on GNSS satellite positioning techniques, quality control of GNSS positioning, integration of sensors and development of innovative solutions considering low-cost navigation sensors (INS and GNSS) for mobile mapping applications and indoor positioning. He authored more than 40 journal papers, 14 book chapters and more than 40 papers in conference proceedings. He is the Chair of the ISPRS Working Group V/3 "Open Source Promotion and Web-based Resource Sharing".

Fabio Dovis is a full professor at the Department of Electronics and Telecommunications of Politecnico di Torino (Turin, Italy), where he coordinates the Navigation Signal Analysis and Simulation – NavSAS - group. His research addresses the design of GNSS receivers, and advanced signal processing for GNSS impairments. He authored more than 70 journal papers and more than 150 papers in conference proceedings. He is member of the IEEE AESS navigation systems panel and he is currently serving in the Council of the US Institute of Navigation. He is a member of the GNSS Scientific Advisory Committee of the European Space Agency and he is also associated to the Italian Space Agency, as scientific support.

ABSTRACT

The issue of multipath and Non-Line-of-Sight (NLoS) interferences has significantly impacted the performance of Global Navigation Satellite System (GNSS) services in various emerging applications, such as autonomous vehicles and smart wearables. Characterizing the statistical pattern for multipath/NLoS interference might enlighten the development of techniques for detecting and mitigating such interferences. For this purpose, this research first introduces a method to estimate pseudorange biases caused by multipath/NLoS using a clustering algorithm. Then, the estimation method for the multipath/NLoS bias is extended to dual-frequency GNSS signals, including Global Positioning System (GPS) L1 C/A and L5. Subsequently, an experiment is carried out to collect and analyze real-world static GNSS data under multipath/NLoS environments. This analysis involved a comparative study of multipath/NLoS patterns using both a geodetic receiver and a smartphone across GPS L1 C/A and L5 signals. The experimental results uncovered some patterns in multipath/NLoS behaviors, offering insights that could potentially guide the development of new algorithms to detect and mitigate such interferences.

I. INTRODUCTION

Global Navigation Satellite System (GNSS) receivers often operate in complex environments where signals transmitted by GNSS satellites are blocked and reflected by objects. These effects violate the fundamental principle of GNSS, which measures the direct distance from the satellite to the receiver, thereby introducing significant errors in Position, Velocity, Timing (PVT) solutions. The phenomenon of receiving reflected GNSS signals is known as multipath and Non-Line-of-Sight (NLoS) McGraw et al. (2020), which are two major issues limiting the wide use of GNSS in emerging applications, ranging from transportation to precision agriculture and smart wearables EU Agency for the Space Program (2024).

The interference from multipath/NLoS is particularly severe in smartphone GNSS units, compared to geodetic GNSS receivers Weng et al. (2023). Geodetic receivers typically feature high-quality, large, fixed-position antennas designed with specific gain patterns that reject signals from below the horizon Volakis et al. (2016); Taghdisi et al. (2021); Groves et al. (2010). In contrast, smartphones operate under more challenging conditions due to several factors:

- **Antenna Attitude**: The orientation of smartphone GNSS antennas frequently changes because of the varying ways users hold their devices. This variability makes it impractical to design antennas with specific gain patterns that reject signals from negative elevations.
- **Antenna Size**: The compact size of smartphones limits the installation of more sophisticated antennas, such as the antenna array and the choke ring antenna, which are crucial for reducing multipath/NLoS interference.
- **Receiver Noise**: The antennas of smartphones generally have higher receiver noise compared to geodetic receivers, further complicating the detection and mitigation of multipath/NLoS interference Zhang et al. (2018).

For both geodetic receivers and smartphones, characterizing multipath and NLoS interferences is crucial for their detection and mitigation. Numerous studies have focused on this characterization, providing valuable insights that reveal the presence of multipath/NLoS and inspire the development of effective mitigation techniques. These studies generally fall into two main categories: multipath/NLoS analysis based on the theoretical signal-processing methods and the statistical model generation based on real-world experiments.

Theoretical signal-processing methods primarily focus on constructing mathematical models of reflected signals during the baseband signal-processing stage Irsigler et al. (2005); Keshvadi et al. (2012); Hegarty et al. (2004); Teunissen and Montenbruck (2017b). This research aims to identify irregular behaviors caused by reflected signals and assess their impact. The influence of these reflected signals is determined by several factors, including the structure of the navigation signal, the design of the code discriminator in the tracking loop, the strength of the reflected signal, and the exact delay of the reflected signal. Typically, the findings from these analyses are presented through multipath error envelopes. These envelopes illustrate the magnitude of code errors induced by specific delays caused by multipath. This visual representation helps in understanding the potential impact of multipath delays on the accuracy of GNSS measurements.

The statistical model approach for multipath/NLoS characterizes the probability distribution of parameters affected by multipath/NLoS based on real-world data collection Sadrieh et al. (2010); Xie and Petovello (2014); Chen (2018). This type of research aims to identify patterns and quantify relationships among various GNSS parameters impacted by multipath, enhancing the development of technologies for detecting and mitigating these effects. Key parameters of interest typically include the Carrier-to-Noise Density Ratio (C/N_0), multipath delay for pseudorange/Doppler, coherent integration time, GNSS receiver's motion, the satellite's elevation angle, and the orbit type of the satellite. This methodology provides an empirical analysis for multipath/NLoS characterization under real-world conditions that often feature challenges such as limited satellite visibility, multiple reflected signals, a variety of reflective media, and high interference from other sources like receiver noise and atmospheric disruptions.

This research addresses the need for a reliable statistical model of the multipath/NLoS effect, focusing on overcoming the limitations of previous studies that lacked effective methods for estimating pseudorange biases caused by multipath/NLoS. Traditional techniques, such as the code-minus-carrier (CMC), often falter under these conditions due to their reliance on the absence of cycle slips, which are challenging to ensure in environments affected by multipath/NLoS. Similarly, methods requiring tracking of satellites at high elevation angles do not perform well in scenarios with restricted satellite visibility, while others depend on complex signal-tracking loops that may not be feasible in all operational contexts.

To address these challenges, this research leveraged a clustering-based technique designed to effectively estimate the multipath/NLoS bias from pseudorange measurements Guo et al. (2024). Furthermore, this multipath/NLoS is developed to apply to both the Global Positioning System (GPS) L1 C/A and L5 signals. Then, this developed approach has been implemented successfully on both a geodetic receiver and a smartphone, enabling the estimation of multipath/NLoS biases for the GPS L1 C/A and L5 signals. Finally, some statistical findings are presented based on comparing the estimated multipath/NLoS biases on pseudorange for different receivers and signals. In summary, the innovations of this research are twofold:

1. A clustering-based algorithm for estimating pseudorange multipath/NLoS biases is extended to both GPS L1 C/A and L5 signals.
2. For both GPS L1 C/A and L5 signals across a geodetic receiver and a smartphone, some empirical behaviors of pseudorange multipath/NLoS biases are observed and concluded.

The remainder of this paper is organized as follows: Section II describes the proposed multipath/NLoS bias estimation method for pseudorange measurement based on a clustering algorithm. Section III introduces the real-world experiment and the statistical conclusion for the pseudorange multipath/NLoS biases based on a Leica GS18 receiver and a Xiaomi Mi 8 smartphone. Eventually, Section IV provides relevant conclusions about this research.

II. GNSS MULTIPATH/NLOS BIAS ESTIMATION FOR PSEUDORANGE

1. Formulation of the proposed leftover term

This subsection recalls the pseudorange observation equation, as outlined in Teunissen and Montenbruck (2017a). The goal is to provide the definition of a proposed leftover term containing the pseudorange biases due to multipath/NLoS, along with other receiver-related error components.

The GNSS receiver generates pseudorange measurement by multiplying the speed of light with the signal travel time from the satellite to the receiver. The pseudorange measurement $p_{r,f}^{s}(t)$ at time t can be modeled as:

$$\begin{aligned} p_{r,f}^{s}(t) = &\left\|\boldsymbol{r}^{s}\left(t\right)-\boldsymbol{r}_{r}\left(t\right)\right\|+\xi_{r}^{s}(t)+I_{f}^{s}(t)+T^{s}(t)-c\left(d_{f}^{s}-dt^{s}(t)+\delta t_{\mathrm{stc}}^{s,\mathrm{rel}}(t)-\delta t_{\mathrm{clk}}^{s,\mathrm{rel}}(t)\right) \\ &+F_{f}^{s}(t)+e_{r,f}^{s}(t)+c\left(d_{r}+dt_{r}(t)\right) \end{aligned} \tag{1}$$

where it should be noted that from here on, superscript s represents the index of a GNSS satellite; subscript r represents the GNSS receiver, subscript f represents the signal type (GPS L1 C/A or L5 in this research) generating pseudorange measurements; and:

- $\boldsymbol{r}^{s}\left(t\right)$ and $\boldsymbol{r}_{r}\left(t\right)$ are the positions of the mass center of the satellite and of the GNSS receiver, respectively. Both are in Earth-Centred Earth-Fixed (ECEF) frame;
- $\xi_{r}^{s}\left(t\right)$ is the antenna phase center correction for both transmitting and receiving antennas;
- $I_{f}^{s}\left(t\right)$ and $T^{s}\left(t\right)$ are the error contributions due to the ionosphere and troposphere delay respectively, expressed in meters. It is noted that $I_{f}^{s}\left(t\right)$ might be different for different signals f;
- c is the speed of light in vacuum;
- d_{f}^{s} and d_{r} are the signal instrumental delay of the satellite and receiver respectively;
- $dt^{s}\left(t\right)$ and $dt_{r}\left(t\right)$ are clock bias of the satellite and receiver respectively;
- $\delta t_{\mathrm{stc}}^{s,\mathrm{rel}}\left(t\right)$ is the delay caused by space-time curvature of the relativistic effect;
- $\delta t_{\mathrm{clk}}^{s,\mathrm{rel}}\left(t\right)$ is satellite clock bias caused by the relativistic effect;
- $F_{f}^{s}\left(t\right)$ is the error contribution due to the multipath/NLoS, expressed in meters;
- $e_{r,f}^{s}\left(t\right)$ is the error contribution due to the receiver noise, expressed in meters;

Meanwhile, the Sagnac effect caused by the earth's rotation should also be compensated for according to Teunissen and Montenbruck (2017a) (Chapter 19.1). Thanks to the advancements in the development of physical models and corrections offered by IGS, all the terms on the first row of the right-hand side of (1) can be computed in a post-processing manner, with relatively high accuracy as outlined in Table 1. The bottom row of (1) is designated as the leftover term $L_{f}^{s}(t)$ of a pseudorange measurement:

$$\begin{aligned} L_{f}^{s}(t) &= F_{f}^{s}(t)+e_{r,f}^{s}(t)+c\left(d_{r}+dt_{r}(t)\right) \\ &= F_{f}^{s}(t)+e_{r,f}^{s}(t)+c\cdot dt_{\mathrm{rcv}}(t) \end{aligned} \tag{2}$$

Since d_{r} and $dt_{r}(t)$ are produced by the GNSS receiver itself, d_{r} remains constant under a specific epoch t for different satellites. Furthermore, the same $dt_{r}(t)$ is also shared for every satellite under a certain epoch t. Therefore, these two terms can be combined as a single term, which is denoted as $dt_{\mathrm{rcv}}(t)$.

The following content of this section will elaborate on the method used in this work to estimate the pseudorange biases caused by multipath and NLoS Guo et al. (2024). First, the leftover term is modeled statistically. Performing a measurement can lead to

Term	Computation method
$p^s_{r,f}(t)$	Pseudorange measurements from the receiver
$\boldsymbol{r}^s(t)$	International GNSS Service (IGS) final precise orbits products
$\boldsymbol{r}_r(t)$	Real-Time Kinematic (RTK) or RTK/Inertial Navigation System (INS) positioning solutions
$\xi^s_r(t)$	Absolute IGS phase center corrections (igs14.atx)
$I^s_f(t)$	Final solution of IGS combined Global Ionospheric Maps (GIMs)
$T^s(t)$	Saastamoinen model
d^s_f	Timing Group Delay (TGD) and Differential Code Bias (DCB) corrections
$dt^s(t)$	Clock biases of the satellites from navigation messages and IGS precise clock products
$\delta t^{s,\mathrm{rel}}_{\mathrm{stc}}(t)$	See Appendix. 1
$\delta t^{s,\mathrm{rel}}_{\mathrm{clk}}(t)$	See Appendix. 2

Table 1: Corrections and models for pseudorange measurement

two outcomes, namely that the measurement is unbiased or that it is biased due to multipath or NLoS. Hence, the leftover term can follow two different probability distributions depending on the outcome. In particular, these distributions will have different mean values since the measurement is biased in one case. This motivates the use of a clustering algorithm to separate and classify leftover terms affected by multipath/NLoS from those that are not. A detailed introduction to a density-based clustering algorithm, namely Density-Based Spatial Clustering of Applications with Noise (DBSCAN), is provided to show its suitability for this task. Then, the procedure of utilizing DBSCAN for multipath/NLoS estimation for the GPS L1 C/A signal is given in detail. Finally, the proposed method estimating the multipath/NLoS bias on the GPS L5 signal is presented.

2. Statistical characterization of the leftover terms

We can start analyzing one by one the components which make up $L^s_f(t)$ in (2), namely:

1. $F^s_f(t)$ is an error contribution on the pseudorange due to the multipath/NLoS. It is important to note that this term is likely different from one satellite to another due to different reflection paths. Furthermore, $F^s_f(t)$ is zero if a satellite is free from both multipath and NLoS phenomena;
2. $e^s_{r,f}(t)$ is the receiver noise which is commonly characterized by a Gaussian distribution with a zero mean and constant variance σ^2 under multipath/NLoS-free conditions Blanch et al. (2012). Although the receiver noise for L1 C/A and L5 signals should have different covariances, these variations are significantly smaller than the biases caused by multipath/NLoS. Therefore, this research does not differentiate between the receiver noise on L1 C/A and L5 signals. Instead, the same sigma value is used for both signal types to simplify the analysis and enhance readability.
3. $dt_{\mathrm{rcv}}(t)$ is the sum of the receiver clock bias and instrumental delay. This term is common to all satellites at a given epoch.

Regardless of the presence of multipath/NLoS, $e^s_{r,f}(t)$ is relatively small compared to $F^s_f(t)$. Typically, in the absence of multipath/NLoS, the range error due to receiver noise is in the order of $\pm 1\,\mathrm{m}$ for a geodetic-quality receiver and antenna Zhang et al. (2018). On the other hand, the ranging bias due to multipath can reach up to about $70\,\mathrm{m}$ for GPS L1 C/A signals with one-chip early-to-late spacing Braasch (1996). Moreover, NLoS conditions may induce biases in pseudorange measurements spanning several kilometers Strode and Groves (2016). Given that $dt_{\mathrm{rcv}}(t)$ and $F^s_f(t)$ are constant for a given epoch, the leftover term $L^s_f(t)$ for a specific satellite can be statistically modeled as Gaussian random variables in both conditions.

$$L^s_f(t) \sim \begin{cases} \mathcal{N}\left(c \cdot dt_{\mathrm{rcv}}(t), \sigma^2\right) & \text{multipath/NLoS-free} \\ \mathcal{N}\left(c \cdot dt_{\mathrm{rcv}}(t) + F^s_f(t), \sigma^2\right) & \text{with multipath/NLoS} \end{cases} \tag{3}$$

The method used in this research leverages the consistency checking principle to detect and estimate multipath/NLoS using leftover terms. This work assumes that at least two satellites are free from the impact of multipath/NLoS. This assumption covers most possible conditions according to Sokhandan et al. (2016). If this assumption fails, the method will be unable to form a cluster consisting of multipath/NLoS-free $L^s_f(t)$. In such a case, the estimation method will declare a failure rather than providing an inaccurate estimate.

In case of no multipath/NLoS, $L^s_f(t)$ is expected to follow the distribution $\mathcal{N}\left(c \cdot dt_{\mathrm{rcv}}(t), \sigma^2\right)$. As a consequence, leftover terms not affected by multipath/NLoS should form a cluster whose span depends on $e^s_{r,f}(t)$. On the other hand, $L^s_f(t)$ should

follow the distribution $\mathcal{N}\left(c \cdot dt_{\mathrm{rcv}}(t) + F_f^s(t), \sigma^2\right)$ in presence of multipath/NLoS. Given that $F_f^s(t)$ is significantly larger than σ, the leftover terms affected by multipath/NLoS will be separated from the main cluster formed by the multipath/NLoS-free leftover terms. Furthermore, it is unlikely that leftover terms impacted by multipath/NLoS can form a common cluster because $F_f^s(t)$ for each satellite has different values due to different reflection paths.

It should be noted that using the described methodology, it could be difficult to identify multipath/NLoS terms $F_f^s(t)$ whose magnitude is not large w.r.t. σ^2. However, as previously recalled, σ^2 is expected to be in the order of $\pm 1\,\mathrm{m}$. This means that $F_f^s(t)$ that are hard to detect will have a minor impact on positioning errors due to their small values. As a result, the main focus of this research is on those sufficiently large values of $F_f^s(t)$ that will lead to considerable loss of accuracy in the navigation solution.

3. DBSCAN, a clustering algorithm for multipath/NLoS estimation

While the previous section motivated the use of a clustering algorithm to detect multipath/NLoS, this section will introduce the specific algorithm used, namely DBSCAN. A suitable parameter selection is also discussed. DBSCAN is a minimum density level estimation that clusters data based on the density. This algorithm first specifies two parameters:

1. minPts: the minimum number of points to form a cluster;
2. ε: the maximum distance between two points to consider them neighbors.

Then, every data point will be classified into one of three types:

1. **Core points**: the data points can find more than minPts neighbors within the radius ε;
2. **Non-core points (border points)**: Within radius ε, the data points can find at least one core point but have no more than minPts neighbors;
3. **Outliers**: the data points do not satisfy neither the definition of core points nor the one of non-core points.

DBSCAN can be described using the flowchart in Figure 1. First, the $\mathrm{RangeQuery}$ function is employed to identify all the neighbors of a specific point. This function finds all the data points in DB whose distance to the current point p is closer than parameter ε. Here, $dist$ is a function used to compute the distance between two data points. Upon identifying a core point, all its neighbors are assigned to the same cluster as that core point. If any of these neighbors is itself a core point, the neighbors of this new core point are classified into the same cluster. This process is iterated until all data points are clustered. Points that do not satisfy the aforementioned conditions are designated as outliers. In particular, the receiver noise variance σ^2 can be used to set the parameter ε, thus controlling the boundary of the main cluster.

DBSCAN is a suitable clustering solution to address the multipath/NLoS problem since the parameter minPts establishes the minimum number of leftover terms $L_f^s(t)$ needed to confirm that they belong to the distribution $\mathcal{N}\left(c \cdot dt_{\mathrm{rcv}}(t), \sigma^2\right)$. Meanwhile, the receiver noise $e_{r,f}^s(t)$ acts as a reference for setting the parameter ε, thus controlling the boundary of the cluster free from multipath/NLoS effects.

4. Estimation of multipath/NLoS bias based on DBSCAN for L1 C/A signal

In total, four steps are involved in estimating the $F_{\mathrm{L1}}^s(t)$ term for the GPS L1 C/A signal. The fundamental concept is to isolate $c \cdot dt_{\mathrm{rcv}}(t)$ from $L_{\mathrm{L1}}^s(t)$ for the pseudorange containing multipath/NLoS using the DBSCAN algorithm. In the initial step all M leftover terms according to (1) at a given epoch are computed:

$$L_{\mathrm{L1}}^s(t), s = 1, ..., M \tag{4}$$

The second step is to run DBSCAN to detect which leftover terms are affected by multipath/NLoS, namely those outside the largest cluster. Sometimes, $L_{\mathrm{L1}}^s(t)$ from different satellites affected by multipath/NLoS could be similar, and potentially form a cluster. However, there is a negligible probability that different multipath/NLoS biases are similar to each other. Therefore, the largest cluster is assumed to contain all the multipath/NLoS-free leftover terms, which are denoted by $\tilde{L}_{\mathrm{L1}}^s(t)$.

The third step is to estimate $dt_{\mathrm{rcv}}(t)$ by computing the mean value of $\tilde{L}_{\mathrm{L1}}^s(t)$:

$$\hat{dt}_{\mathrm{rcv}}(t) = mean\left(\tilde{L}_{\mathrm{L1}}^s(t)\right) \tag{5}$$

These $\tilde{L}_{\mathrm{L1}}^s(t)$ should have multipath/NLoS terms equal to zero. Thus, the mean operation has the effect of mitigating the noise

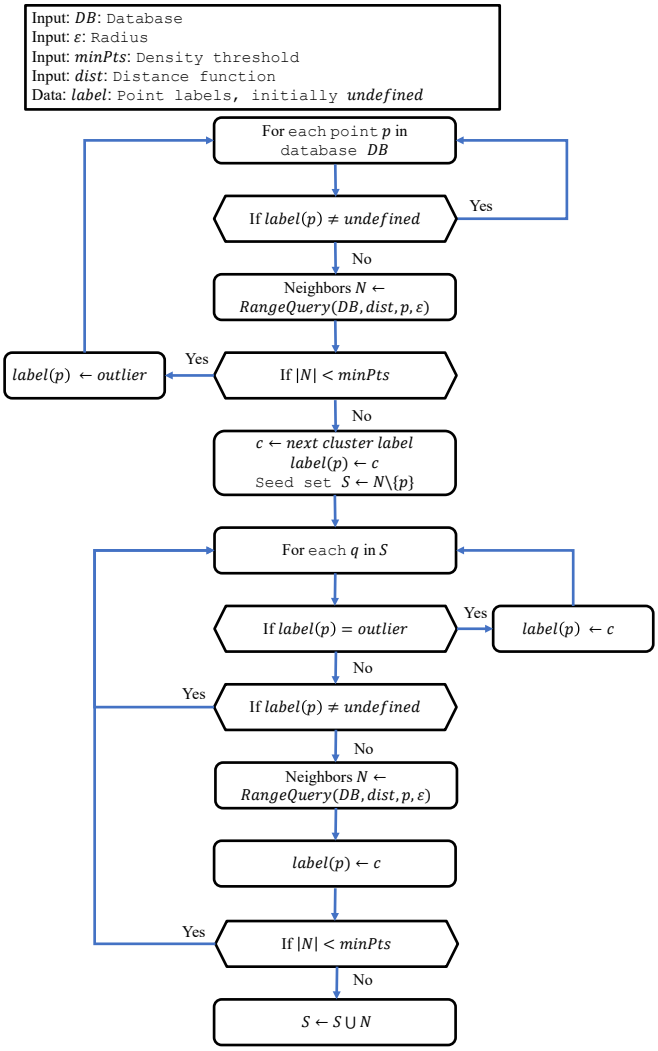

Figure 1: Flowchart of the DBSCAN algorithm

to estimate the common term due to the receiver clock.

The final step is to use the estimate of $dt_{\mathrm{rcv}}(t)$ and remove it from the leftover terms outside the main cluster. By this way, the effect due to the receiver clock is removed, and the biases on pseudorange measurements due to multipath/NLoS can be estimated:

$$\hat{F}^s_{\mathrm{L1}}(t) = L^s_{\mathrm{L1}}(t) - c \cdot \hat{dt}_{\mathrm{rcv}}(t),\ \forall s \text{ out of the largest cluster} \tag{6}$$

5. Estimation of multipath/NLoS bias for L5 signal

Estimating the biases using the proposed clustering method is more challenging for L5 than for L1 C/A signals due to fewer satellites transmitting L5—only 17 out of 31 GPS satellites. This reduces satellite visibility, which is crucial for effective clustering in environments affected by multipath/NLoS. However, as indicated by (6), the key to estimating $\hat{F}^s_f(t)$ lies in determining the value of $\hat{dt}_{\mathrm{rcv}}(t)$, which is identical for both L1 C/A and L5 signals. Therefore, the multipath/NLoS estimation can directly utilize the estimated $\hat{dt}_{\mathrm{rcv}}(t)$ rather than relying on the DBSCAN clustering algorithm.

The process begins by calculating the leftover terms for the L5 signals in the same manner as for the L1 C/A signals according to (2):

$$L^s_{\mathrm{L5}}(t), s = 1, ..., M \tag{7}$$

Subsequently, the $\hat{dt}_{\mathrm{rcv}}(t)$ estimated based on the L1 C/A measurements in (5) is applied to (2), resulting in the computation of the sum $F^s_{\mathrm{L5}}(t) + e^s_{r,\mathrm{L5}}(t)$ as:

$$F^s_{\mathrm{L5}}(t) + e^s_{r,\mathrm{L5}}(t) = L^s_{\mathrm{L5}}(t) - c \cdot \hat{dt}_{\mathrm{rcv}}(t) \tag{8}$$

Then, a threshold $F^{\mathrm{th}}_{\mathrm{L5}}$ for computed $F^s_{\mathrm{L5}}(t) + e^s_{r,\mathrm{L5}}(t)$ is set based on the receiver noise level. If the sum $F^s_{\mathrm{L5}}(t) + e^s_{r,\mathrm{L5}}(t)$ falls below these thresholds, it is considered to be influenced solely by receiver noise, without the impact of multipath/NLoS. Conversely, if the sum $F^s_{\mathrm{L5}}(t) + e^s_{r,\mathrm{L5}}(t)$ exceeds these thresholds, it is presumed to be dominated by multipath/NLoS and is thus estimated as the bias due to these effects. This multipath/NLoS estimation process can be described as:

$$\hat{F}^s_{\mathrm{L5}}(t) := \begin{cases} F^s_{\mathrm{L5}}(t) + e^s_{r,\mathrm{L5}}(t) & \text{for } F^s_{\mathrm{L5}}(t) + e^s_{r,\mathrm{L5}}(t) \geq F^{\mathrm{th}}_{\mathrm{L5}} \\ 0 & \text{for } F^s_{\mathrm{L5}}(t) + e^s_{r,\mathrm{L5}}(t) < F^{\mathrm{th}}_{\mathrm{L5}} \end{cases} \tag{9}$$

III. EXPERIMENT AND DISCUSSION

1. Experimental setup

A real-world experiment to evaluate multipath effects was conducted at the Politecnico di Torino, Italy, as illustrated in Figure 2. For this experiment, a Leica GS18 receiver and a Xiaomi Mi 8 smartphone were used to collect raw GNSS measurements of the GPS L1 C/A and GPS L5 signals at a fixed position, with a sampling rate of $1\,\mathrm{Hz}$. The data collection phase lasted approximately 4 hours, amounting to 15000 epochs. The sky plots for both the Leica receiver and the Mi 8, which displays the carrier-power-to-noise-density ratio (C/N_0), is shown in Figure 3. Variations in the C/N_0 values could indicate significant multipath/NLoS interference.

The precise locations of both the Leica receiver and the Mi 8 were georeferenced using RTK solutions from the Leica receiver to establish the ground truth for the test. Only the fixed RTK solutions were selected and averaged to determine the ground truth. Although the antenna phase centers of the Leica receiver and Mi 8 are misaligned by approximately $10\,\mathrm{cm}$, this research primarily focuses on the multipath/NLoS biases, which typically extend to tens of meters. Therefore, this misalignment is considered negligible.

To determine the $L^s_f(t)$ values for the pseudorange measurements, all necessary corrections and models, as detailed in Table 1, were computed. Regarding the configuration of the DBSCAN algorithm, the settings for the parameters $minPts$ and ε are provided in Table 2.

	$minPts$	ε
Leica	2	$2\,\mathrm{m}$
Mi 8	2	$10\,\mathrm{m}$

Table 2: Parameter settings for DBSCAN

Given the typically limited satellite visibility in urban environments, the $minPts$ parameter was set to 2, ensuring that at least two points are necessary to confirm membership in the same cluster. The ε parameter, which represents the maximum allowable distance between two points in the same cluster, was specifically adapted to our study's context. For the Leica receiver and the Mi 8, this maximum distance of the distribution $\mathcal{N}\left(c \cdot dt_{\mathrm{rcv}}(t), \sigma^2\right)$ is dependent on the particular variance σ^2, which is associated with their own receiver noise. From our open sky static data campaign, we determined that the 3σ values of receiver noise are approximately $1\,\mathrm{m}$ for the Leica receiver and $5\,\mathrm{m}$ for the Mi 8. Consequently, we set ε to two times the 3σ value for each device.

2. Multipath/NLoS Estimation using DBSCAN

This section will first detail the multipath/NLoS estimation procedures and their results for the L1 C/A signal on both the Leica receiver and the Mi 8. Subsequently, it will present the multipath/NLoS estimation results for the L5 signal, enabling a comprehensive comparison.

Figure 2: GNSS data collection scenarios with intensive multipath/NLoS.

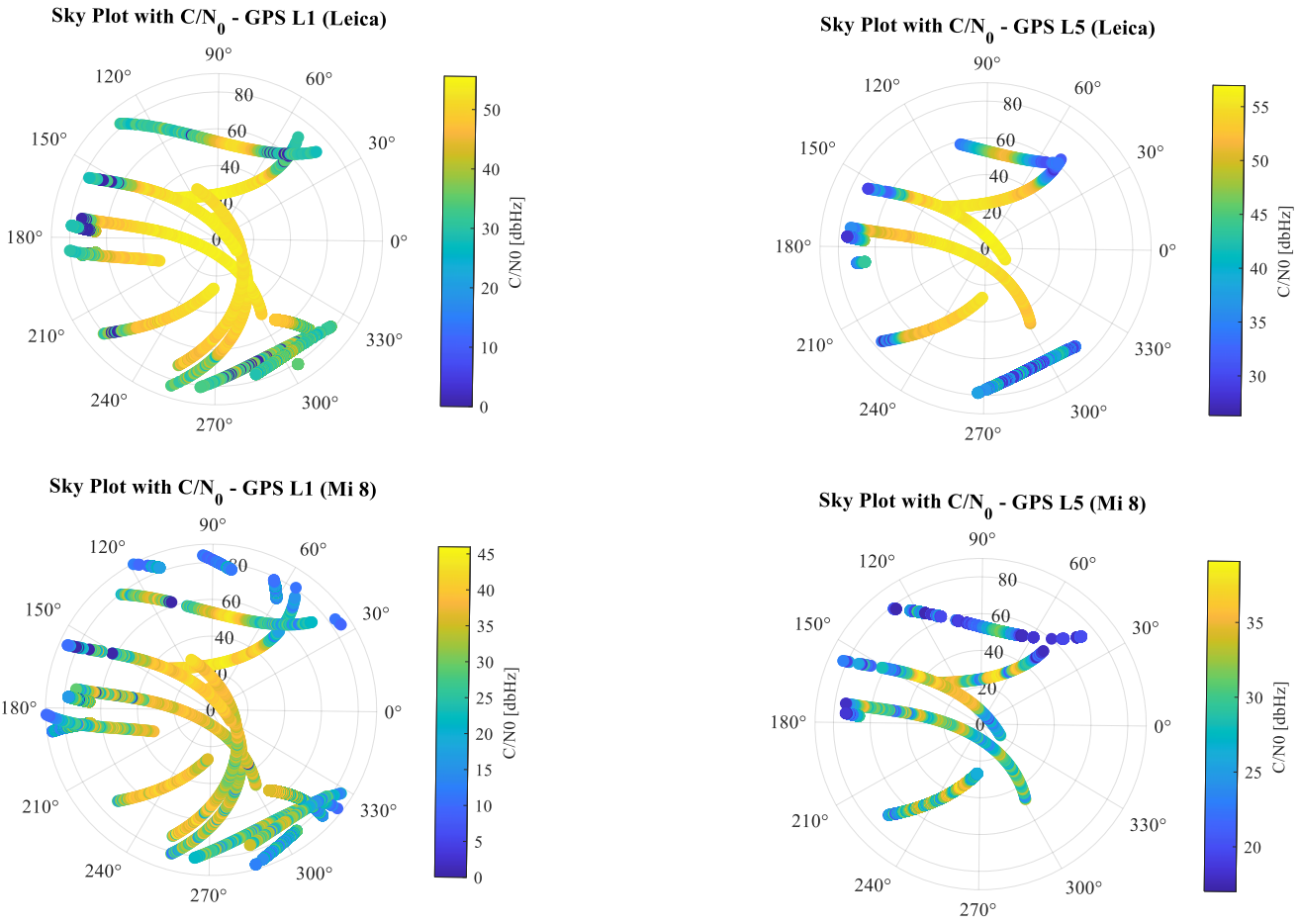

Figure 3: Sky plots with the corresponding C/N_0.

For the L1 C/A signal, as a preliminary step, all corrections and models outlined in Table 1 were applied to calculate the pseudorange leftover terms for both the Leica receiver and the Mi 8. Figure 4 displays the resulting $L^s_{\mathrm{L1}}(t)$ values for GPS

L1 C/A signals, which are color-coded to differentiate the Pseudo Random Noise (PRN) of each satellite. For both the Leica receiver and the Mi 8, the majority of the $L^s_{\mathrm{L1}}(t)$ values follow a similar pattern, suggesting that they are primarily influenced by $c \cdot dt_{\mathrm{rcv}}(t)$. However, deviations in certain $L^s_{\mathrm{L1}}(t)$ values from this general trend indicate the presence of significant biases $F^s_{\mathrm{L1}}(t)$, which are likely due to multipath/NLoS effects.

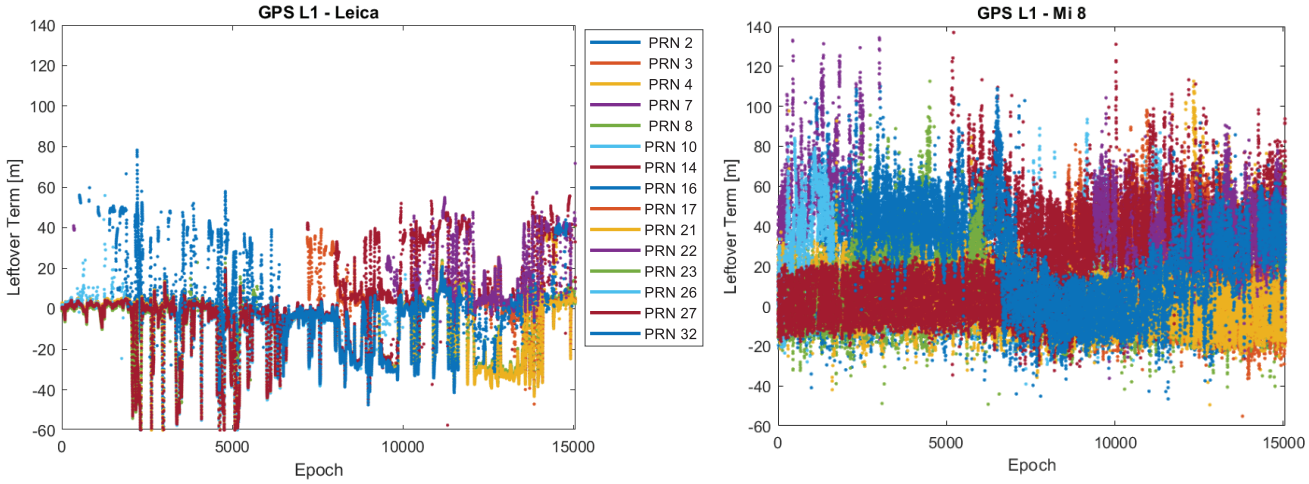

Figure 4: Computed leftover terms $L^s_{\mathrm{L1}}(t)$ for Leica receiver and Mi 8 (GPS L1 C/A).

Subsequently, for GPS L1 C/A signals, Figure 5 displays all the $\tilde{L}^s_{\mathrm{L1}}(t)$ values located within the largest cluster, as identified by the DBSCAN algorithm. The estimated $c \cdot \hat{dt}_{\mathrm{rcv}}(t)$ is computed by averaging these $\tilde{L}^s_{\mathrm{L1}}(t)$ values, which are recognized as being unaffected by multipath/NLoS interference.

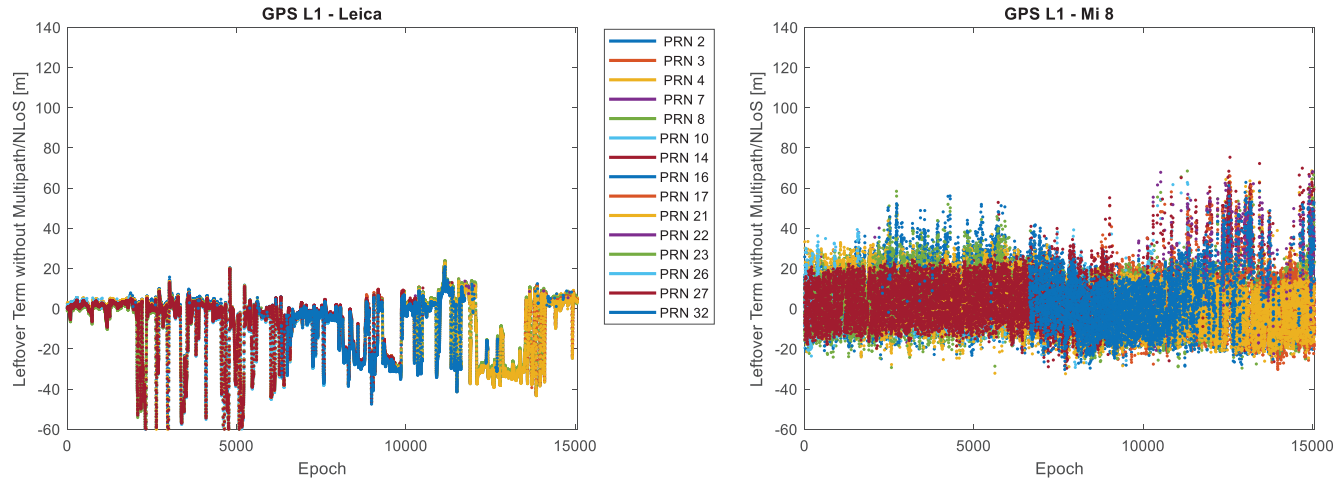

Figure 5: Leftover terms $\tilde{L}^s_{\mathrm{L1}}(t)$ in the largest cluster determined by DBSCAN for Leica receiver and Mi 8 (GPS L1 C/A).

Given the estimated $c \cdot \hat{dt}_{\mathrm{rcv}}(t)$, the $\hat{F}^s_{\mathrm{L1}}(t)$ values for the leftover terms not included in the largest cluster can be determined using (6). These values are illustrated in the left part of Figure 6.

For the Mi 8, receiver noise typically ranges from $-5\,\mathrm{m}$ to $5\,\mathrm{m}$, which needs to be accounted for when estimating $\hat{F}^s_{\mathrm{L1}}(t)$. Given that receiver noise can usually be modeled as a random variable with a zero mean, this study employs a Gaussian-weighted moving average filter with a window size of 10 on the leftover term $\tilde{L}^s_{\mathrm{L1}}(t)$. This filter effectively mitigates the impact of the receiver noise $e^s_{r,f}(t)$, thus aiding in the more accurate computation of $\hat{F}^s_{\mathrm{L1}}(t)$. For the Leica receiver, however, such smoothing is not required due to the significantly lower receiver noise levels.

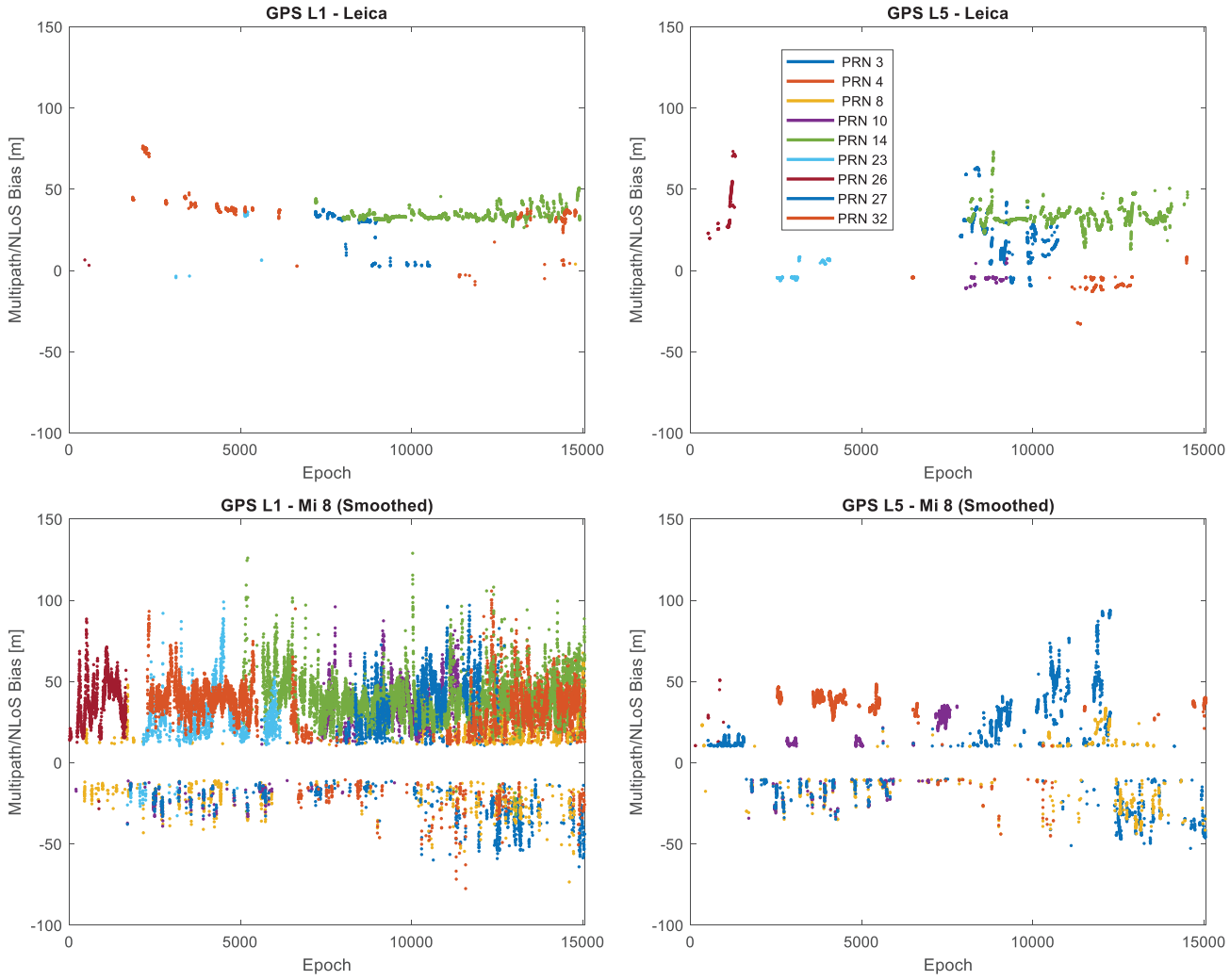

Figure 6: Estimated multipath/NLoS bias $\hat{F}_f^s(t)$ on pseudorange for Leica receiver and Mi 8 (GPS L1 C/A and GPS L5).

After obtaining the $\hat{F}^s_{\mathrm{L1}}(t)$ values, it is crucial to verify the reliability of these estimates. The difficulty of such a verification lies in the fact that ground truth values are only accessible for positioning results but not for the receiver clock bias $dt_r(t)$ in (1). The accurate estimation of $dt_r(t)$ is even more challenging under a multipath/NLoS condition with biased GNSS measurements.

Therefore, to validate the accuracy of the estimated multipath/NLoS biases, we assess the effectiveness of the correction at the PVT level. This is done by comparing the accuracy of PVT solutions obtained from pseudoranges with and without the corrections for multipath/NLoS biases. To facilitate this comparison, new positioning results are computed using a fresh GNSS dataset. This dataset is generated by compensating for the $\hat{F}^s_{\mathrm{L1}}(t)$ in the pseudorange measurements, specifically by subtracting the estimated $\hat{F}^s_{\mathrm{L1}}(t)$ from the corresponding pseudorange values.

Figure 7 displays the time series of positioning errors in both the horizontal and vertical directions, before and after applying multipath/NLoS compensation. It is observed that the positioning errors are generally smaller in magnitude than the estimated $\hat{F}^s_{\mathrm{L1}}(t)$ values for the dataset without multipath/NLoS compensation. This suggests that the computed $\hat{F}^s_{\mathrm{L1}}(t)$ values accurately reflect the actual pseudorange biases resulting from multipath/NLoS effects. The Cumulative Density Functions (CDFs) depicted in Figure 8 illustrates the distribution of positioning errors. This figure plays a crucial role in assessing the improvements in positioning accuracy following the compensation for multipath/NLoS effects.

The final step of this section involves estimating the multipath/NLoS biases for L5 signals according to the procedure illustrated in Section II.5. Thresholds $F^{\mathrm{th}}_{\mathrm{L5}}$ of $1\,\mathrm{m}$ for the Leica receiver and $5\,\mathrm{m}$ for the Mi 8 are then set based on their respective noise

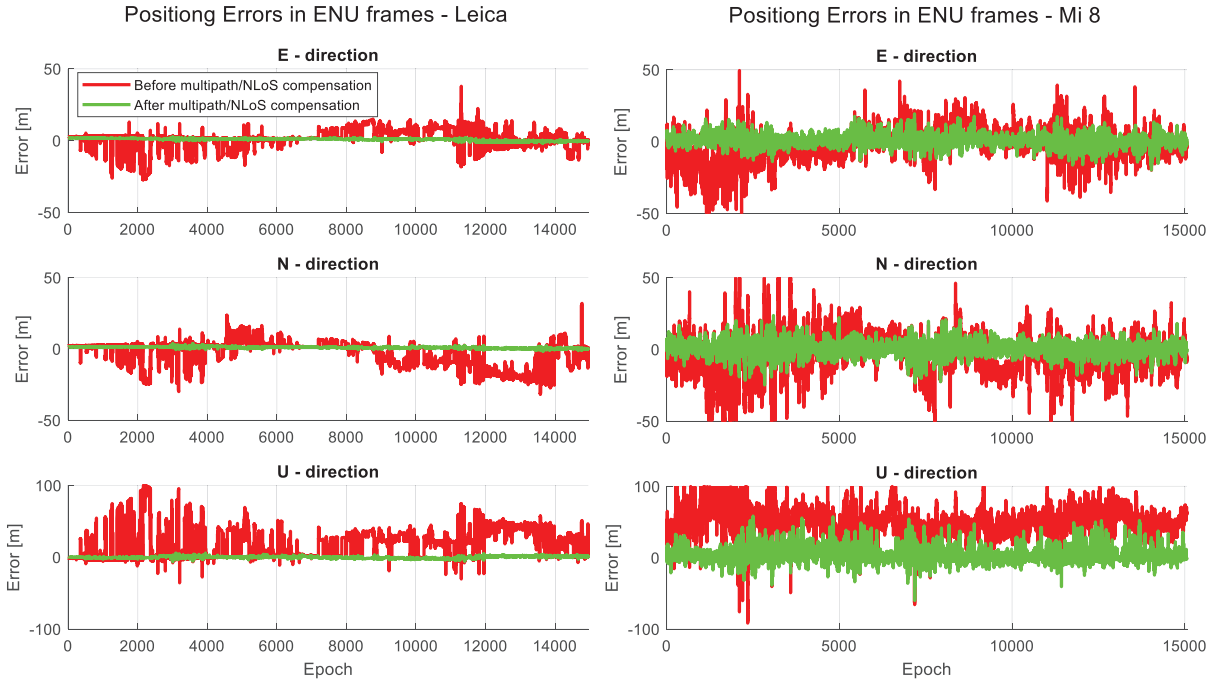

Figure 7: Positioning error time series before and after pseudorange multipath/NLoS compensation in East, North, and Up directions for Leica and Mi 8.

levels. The right part of Figure 6 shows the estimated multipath/NLoS biases for both the Leica receiver and the Mi 8 on L5 pseudorange. Additionally, a smoothing operation is applied to the L5 signals, following the same parameters as set for the L1 C/A signals.

3. Disussion

This section aims to provide a detailed comparison of multipath/NLoS characteristics across different receivers and frequency bands. All subsequent analyses are based on multipath/NLoS-related parameters for both the Leica receiver and the Mi 8, as well as for the dual frequencies L1 C/A and L5.

Firstly, Figure 9 illustrates the duration of multipath/NLoS interference as a percentage of the total signal tracking period for each PRN code. Additionally, the elevation angle of each satellite is included for reference. From this figure, several empirical conclusions can be drawn:

- For both the Leica receiver and the Mi 8, tracking the L1 C/A signal is generally easier than tracking the L5, particularly under conditions of low satellite elevations where multipath/NLoS is more prevalent. The L1 C/A signal tends to experience more frequent multipath interference due to its higher tracking sensitivity at low elevations.
- For the Leica receiver, when both L1 C/A and L5 are tracked, multipath/NLoS incidents occur more frequently on the L5 signal than on the L1 C/A. This phenomenon is particularly obvious by observing the PRNs G10, G23, G26, G27, and G32.
- The Mi 8 displays more complex multipath/NLoS characteristics, which do not readily conform to a simple pattern or rule.

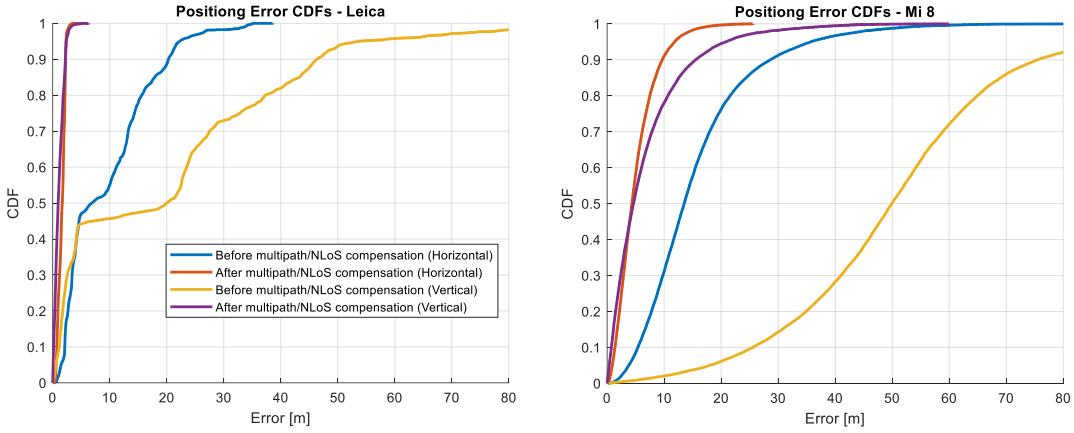

Figure 8: CDFs of positioning errors before and after pseudorange multipath/NLoS compensation in horizontal and vertical directions.

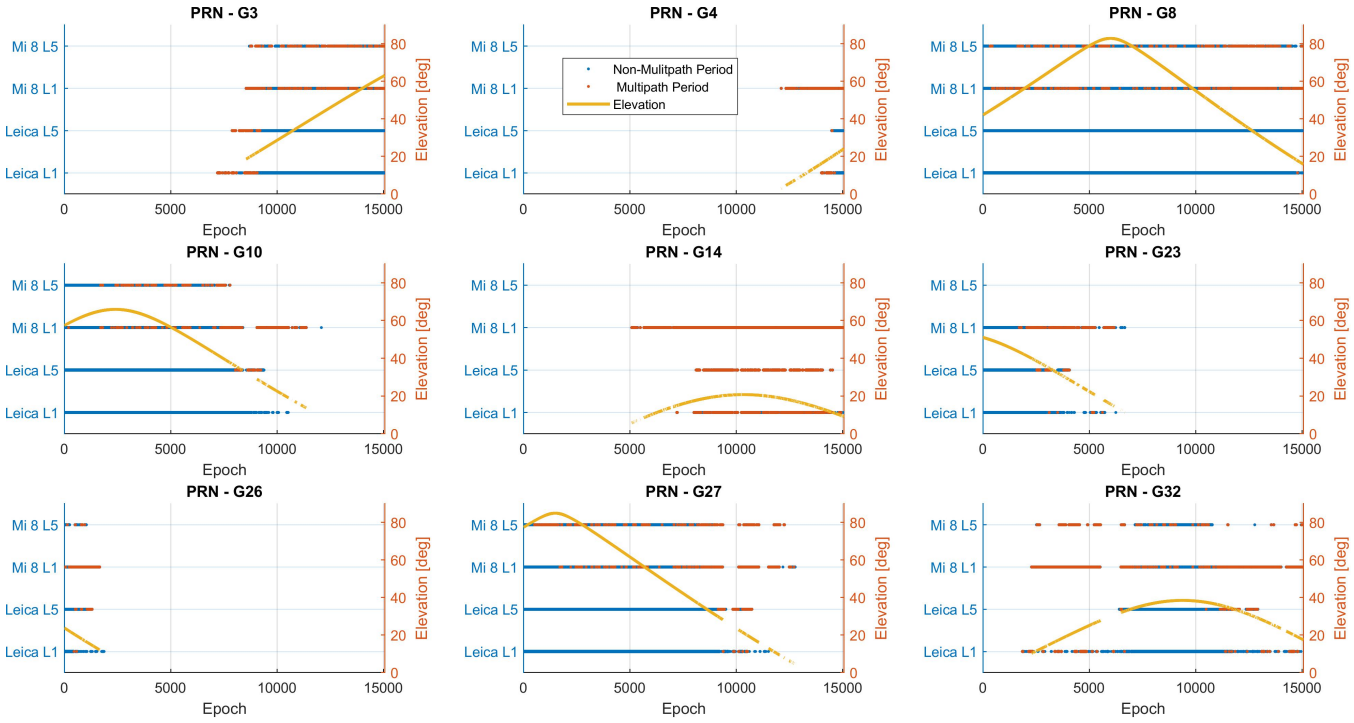

Figure 9: Satellite visibility and multipath/NLoS conditions.

As depicted in Figure 6, multipath/NLoS biases exhibit slow-changing trends. Consequently, Figure 10 is designed to illustrate the stability of these biases by plotting the first-order differences of the estimated multipath/NLoS biases. From this analysis,

several observations can be noted:

- For the Leica receiver, the first-order differences in multipath/NLoS biases for the L1 frequency are generally larger than those for L5. However, L5 exhibits some significant outliers, with differences ranging from $10\,\mathrm{m}$ to $20\,\mathrm{m}$.
- For the Mi 8, the L5 frequency shows better stability in multipath/NLoS biases, with smaller differences compared to L1 C/A.
- When comparing the Leica receiver with the Mi 8, the stability of multipath/NLoS biases on L5 is generally better across both devices, except for the notable outliers in the Leica receiver's L5 data.

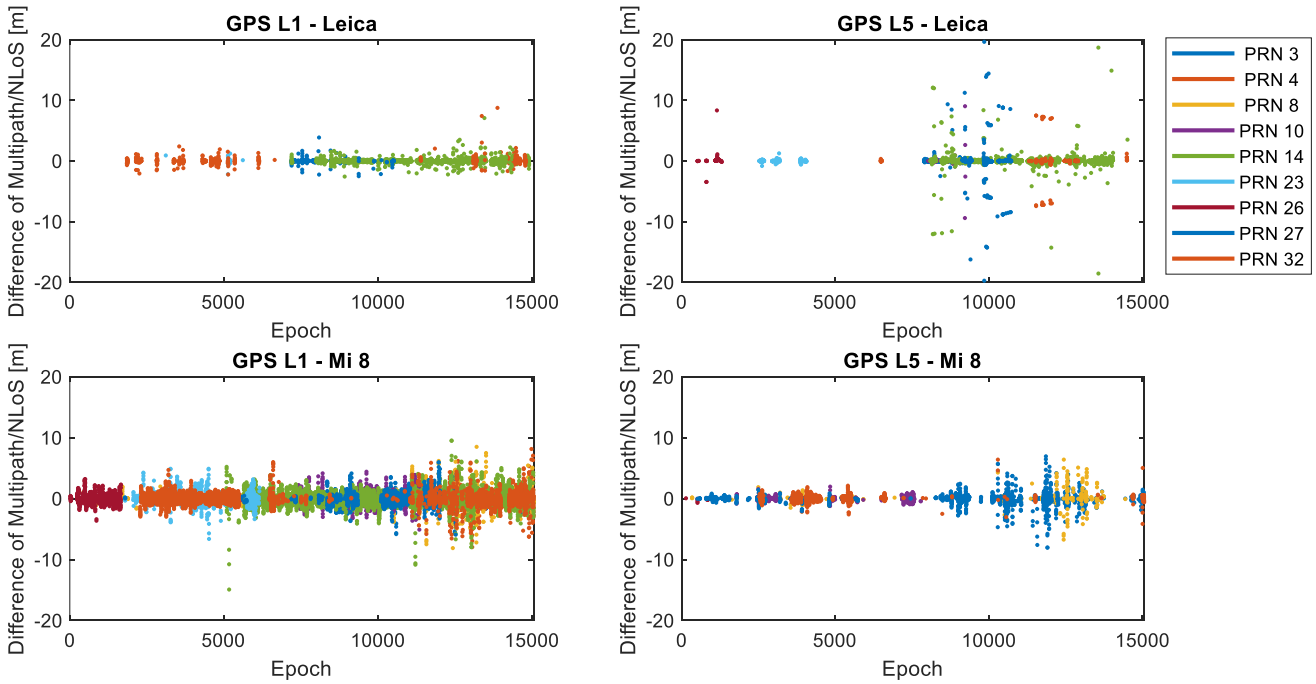

Figure 10: First-order difference of estimated multipath/NLoS biases.

This experiment conducts a separate comparison of multipath/NLoS bias values for the Leica receiver and the Mi 8, presented in Figures 11 and 12, respectively, to ensure clarity in the visual presentation. For both receivers, there is a significant correlation between the L1 C/A and L5 signals concerning the occurrence and magnitude of multipath/NLoS biases. This correlation is evident as the multipath/NLoS biases for both L1 C/A and L5 signals at the same epochs show approximately equal values. This finding suggests that dual-frequency data may be effectively utilized to detect and mitigate multipath/NLoS effects.

IV. CONCLUSION

This paper introduces a post-processing method for estimating pseudorange bias due to multipath/NLoS using the DBSCAN clustering algorithm. A static collection of GNSS raw measurements involving a geodetic receiver and a smartphone was conducted for both GPS L1 C/A and L5 signals in a multipath/NLoS scenario. The proposed method was then applied to this dataset to statistically characterize the multipath/NLoS bias on the pseudorange measurements.

Some conclusions can be drawn based on the experimental results. Firstly, the reliability of the estimated biases was validated by assessing the positioning accuracy of a Least-Squares (LS) algorithm using pseudoranges compensated for these estimated multipath/NLoS biases. The analysis identified several key phenomena regarding multipath/NLoS for the geodetic receiver (Leica GS18) and the smartphone (Xiaomi Mi 8) across GPS L1 C/A and L5 signals:

1. The L1 C/A signal exhibits better trackability under low-elevation conditions but with significant multipath/NLoS for both types of receivers.
2. The Leica receiver is more susceptible to multipath/NLoS on the L5 signal than on the L1 C/A, a trend not observed in the Mi 8.

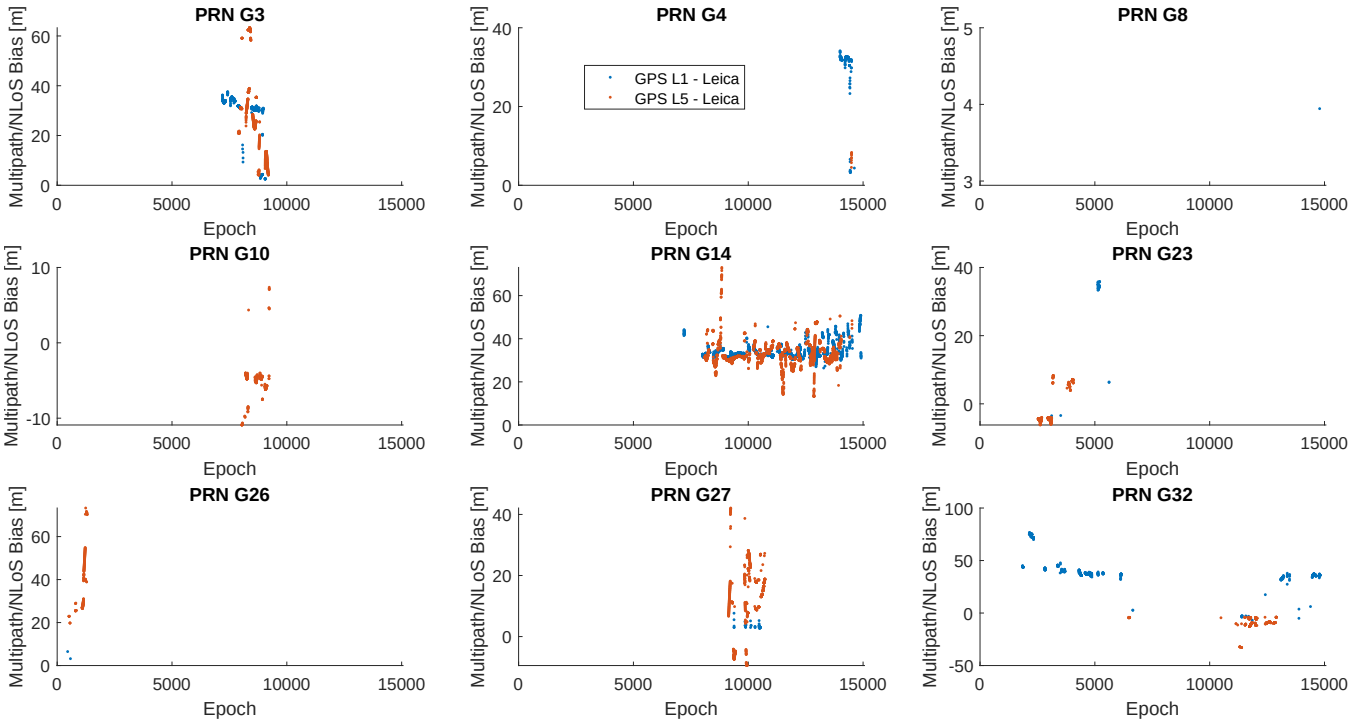

Figure 11: Comparison of estimated multipath/NLoS biases for Leica (GPS L1 C/A and L5).

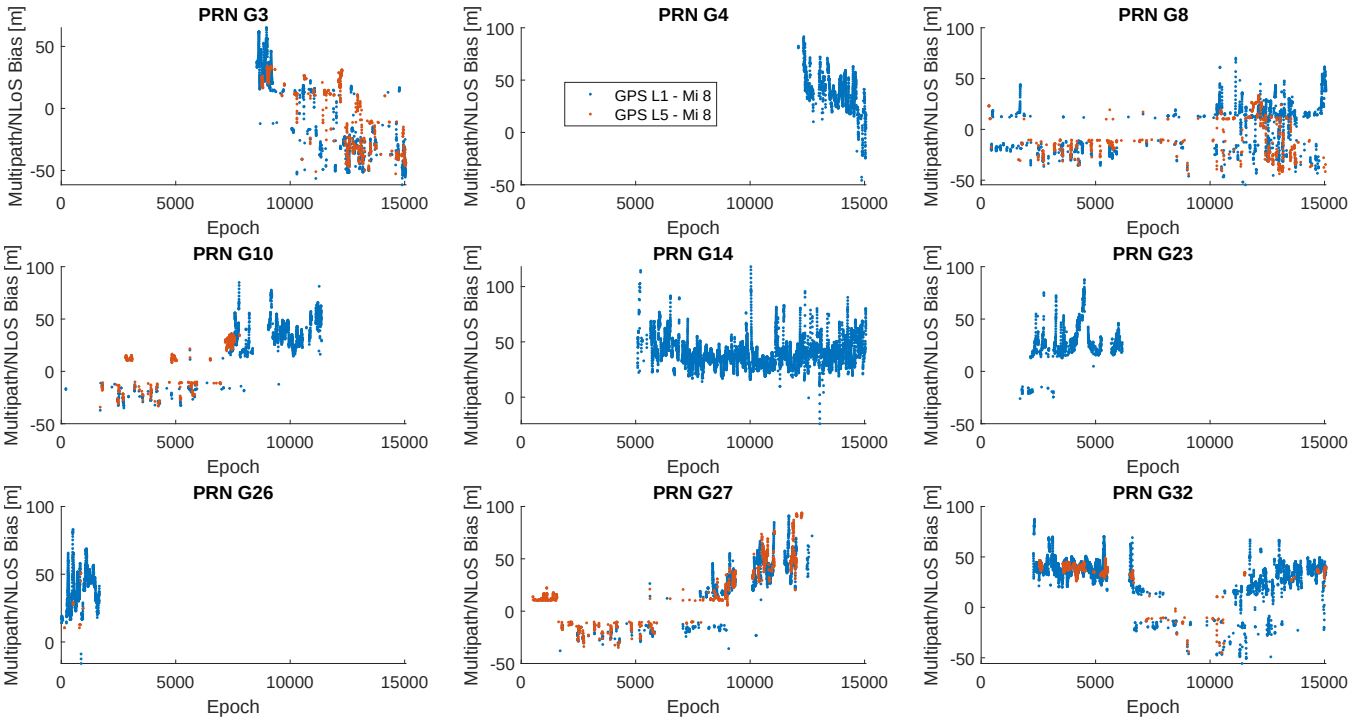

Figure 12: Comparison of estimated multipath/NLoS biases for Mi 8 (GPS L1 C/A and L5).

3. Generally, the first-order difference of multipath/NLoS biases, indicative of bias stability, is greater for the Mi 8 and L1 C/A signals compared to the Leica receiver and L5 signal, although some outliers were noted for the Leica receiver on the L5 signal.

4. A strong correlation is evident between the multipath/NLoS biases on pseudorange measurements for both receivers, demonstrating similar bias values across frequencies.

These findings highlight specific patterns in multipath/NLoS biases for dual-frequency signals and different receiver types, potentially guiding future research toward developing more effective techniques for detecting and mitigating multipath/NLoS.

V. APPENDIX

1. Shapiro Effect Correction

Earth's gravitational field causes the Shapiro effect, which results in a time delay for GNSS signal propagation. The correction for the Shapiro effect can be compensated by:

$$\delta t_{\mathrm{stc}}^{s,\mathrm{rel}} = \frac{2\mu}{c^3} \ln \left(\frac{\|\boldsymbol{r}^s\| + \|\boldsymbol{r}_r\| + \rho_r^s}{\|\boldsymbol{r}^s\| + \|\boldsymbol{r}_r\| - \rho_r^s} \right) \tag{10}$$

where

- μ is the gravitational constant of Earth.

2. Relativistic Clock Correction

The relativity affects the satellite clock through both the satellite motion and the unsteady gravitation field. Although the oscillator frequency of the satellite clock has been intentionally offset to compensate for the relativistic effect, the elliptical satellite orbits cause deviations to the set offset. The compensation due to the orbit eccentricity can be calculated from

$$\delta t_{\mathrm{clk}}^{s,\mathrm{rel}} = -\frac{2}{c^2} \sqrt{a\mu} e \sin E \tag{11}$$

- a is the orbit semimajor axis;
- e is the orbit eccentricity;
- E is the eccentric anomaly of the satellite.

ACKNOWLEDGEMENTS

The Ph.D. grant of Yihan Guo by the Chinese Scholarship Council (CSC)[1].

REFERENCES

Blanch, J., Walter, T., Enge, P., Lee, Y., Pervan, B., Rippl, M., and Spletter, A. (2012). Advanced RAIM user algorithm description: Integrity support message processing, fault detection, exclusion, and protection level calculation. In *Proceedings of the 25th International Technical Meeting of The Satellite Division of the Institute of Navigation (ION GNSS 2012)*, pages 2828–2849.

Braasch, M. S. (1996). GPS multipath model validation. In *Proceedings of Position, Location and Navigation Symposium-PLANS'96*, pages 672–678. IEEE.

Chen, X. (2018). Statistical multipath model comparative analysis of different gnss orbits in static urban canyon environment. *Advances in Space Research*, 62(5):1034–1048.

EU Agency for the Space Program (2024). EUSPA EO and GNSS Market Report 2024. `https://www.euspa.europa.eu/sites/default/files/euspa_market_report_2024.pdf`.

Groves, P. D., Jiang, Z., Skelton, B., Cross, P. A., Lau, L., Adane, Y., and Kale, I. (2010). Novel multipath mitigation methods using a dual-polarization antenna. In *Proceedings of the 23rd International Technical Meeting of The Satellite Division of the Institute of Navigation (ION GNSS 2010)*, pages 140–151.

Guo, Y., Zocca, S., Dabove, P., and Dovis, F. (2024). A post-processing multipath/nlos bias estimation method based on dbscan. *Sensors*, 24(8):2611.

[1] https://www.csc.edu.cn/

Hegarty, C., Tran, M., and Betz, J. W. (2004). Multipath performance of the new gnss signals. In *Proceedings of the 2004 National Technical Meeting of The Institute of Navigation*, pages 333–342.

Irsigler, M., Avila-Rodriguez, J. A., and Hein, G. W. (2005). Criteria for gnss multipath performance assessment. In *Proceedings of the 18th International Technical Meeting of the Satellite Division of The Institute of Navigation (ION GNSS 2005)*, pages 2166–2177.

Keshvadi, H., Broumandan, A., and Lachapelle, G. (2012). Spatial characterization of gnss multipath channels. *International Journal of Antennas and Propagation*, 2012(1):236464.

McGraw, G. A., Groves, P. D., and Ashman, B. W. (2020). Robust positioning in the presence of multipath and NLOS GNSS signals. *Position, navigation, and timing technologies in the 21st century: integrated satellite navigation, sensor systems, and civil applications*, 1:551–589.

Sadrieh, S. N., Broumandan, A., and Lachapelle, G. (2010). Spatial/temporal characterization of the gnss multipath fading channels. In *Proceedings of the 23rd International Technical Meeting of the Satellite Division of The Institute of Navigation (ION GNSS 2010)*, pages 393–401.

Sokhandan, N., Curran, J. T., Broumandan, A., and Lachapelle, G. (2016). An advanced GNSS code multipath detection and estimation algorithm. *GPS solutions*, 20:627–640.

Strode, P. R. and Groves, P. D. (2016). GNSS multipath detection using three-frequency signal-to-noise measurements. *GPS solutions*, 20:399–412.

Taghdisi, E., Ghaffarian, M. S., and Mirzavand, R. (2021). Low-profile substrate integrated choke rings for GNSS multipath mitigation. *IEEE Transactions on Antennas and Propagation*, 70(3):1706–1718.

Teunissen, P. J. and Montenbruck, O. (2017a). *Springer handbook of global navigation satellite systems*. Springer.

Teunissen, P. J. and Montenbruck, O. (2017b). *Springer handbook of global navigation satellite systems, Chapter 15*. Springer.

Volakis, J. L., O'Brien, A. J., and Chen, C.-C. (2016). Small and adaptive antennas and arrays for GNSS applications. *Proceedings of the IEEE*, 104(6):1221–1232.

Weng, D., Hou, Z., Meng, Y., Cai, M., and Chan, Y. (2023). Characterization and mitigation of urban gnss multipath effects on smartphones. *Measurement*, 223:113766.

Xie, P. and Petovello, M. G. (2014). Measuring GNSS multipath distributions in urban canyon environments. *IEEE Transactions on Instrumentation and Measurement*, 64(2):366–377.

Zhang, X., Tao, X., Zhu, F., Shi, X., and Wang, F. (2018). Quality assessment of GNSS observations from an Android N smartphone and positioning performance analysis using time-differenced filtering approach. *Gps Solutions*, 22:1–11.